JOURNAL OF GEOPHYSICAL RESEARCH, VOL. 102, NO. C8, PAGES 18,627–18,639, AUGUST 15, 1997

Seasonal variability of sea surface $\Delta^{14}C$ in the equatorial Pacific in an ocean circulation model

Keith B. Rodgers and Mark A. Cane

Lamont-Doherty Earth Observatory of Columbia University, Palisades, New York

Daniel P. Schrag

Department of Geological Sciences, Princeton University, Princeton, New Jersey

Abstract. The object of this modeling study is to identify the physical mechanisms responsible for seasonal variability in sea surface $\Delta^{14}C$ for the equatorial Pacific Ocean. Analyses of $\Delta^{14}C$ in corals from Guam, Galapagos, Fanning, and Canton reveal seasonal variability between 30 and 50 per mil during the 1970s and early 1980s. Given that this variability occurs on seasonal timescales, whereas air-sea isotopic equilibration occurs on a timescale of 5 to 10 years, the variability must be due to seasonal variability in the physical circulation of the ocean. We use the primitive equation ocean circulation model of *Gent and Cane* [1989], along with the hybrid mixed layer model of *Chen et al.* [1994a], to study the dynamical mechanisms responsible. Upwelling in the eastern equatorial Pacific brings up $\Delta^{14}C$-depleted waters, and air-sea exchange creates high $\Delta^{14}C$ in the western equatorial Pacific, establishing horizontal gradients in sea surface $\Delta^{14}C$. Seasonally varying lateral advection, acting on these gradients, is the dominant mechanism for $\Delta^{14}C$ variability in the equatorial Pacific. In addition to the runs which were forced with seasonally varying winds, a run which used interannual winds between 1971 and 1985 was performed. The substantial interannual $\Delta^{14}C$ variability present in this run is associated with advective anomalies in the equatorial waveguide.

Introduction

This investigation addresses the seasonal variability of $\Delta^{14}C$ for the surface waters of the equatorial Pacific. $\Delta^{14}C$ has been introduced as a tracer into the primitive equation ocean general circulation model (GCM) of *Gent and Cane* [1989]. The model is configured for an equatorial Pacific domain and is run at high resolution so as to resolve changes in circulation associated with the seasonal cycle.

Our modeling study was initially motivated by a desire to understand the seasonal $\Delta^{14}C$ variability recorded by corals in the tropical Pacific. *Brown et al.* [1993] measured seasonal variability at Galapagos of the order of 30 to 40 per mil for corals which grew over the interval 1970-1974 and in excess of 50 per mil during the 1972-1972 El Niño. *Moore et al.* [1997] found seasonal variability as large as 40 per mil for Guam corals from the late 1970s and early 1980s. *Druffel* [1987] measured 6-month averages of coral $\Delta^{14}C$ at both Canton and Fanning from the early 1970s that revealed variability of order 40 per mil. At each of the locations where the seasonal variability of coral $\Delta^{14}C$ has been measured in the equatorial Pacific, it has been between 30 and 50 per mil.

The physical processes which can contribute to this variability in sea surface $\Delta^{14}C$ include upwelling and lateral advection. These mechanisms each have a preferred phase with respect to the march of the seasons and are controlled by seasonal changes in wind forcing. Air-sea exchange can also contribute to variability, but because isotopic equilibration typically occurs on a timescale of 5 to 10 years, it is unlikely to be as important as the other mechanisms on seasonal timescales. As we are focusing on the seasonal cycle in surface waters, we will neglect radioactive decay in our discussion, since its characteristic timescale for changes is much longer. Over 1 year of model integration, radioactive decay will cause the $\Delta^{14}C$ of thermocline waters to decrease only 0.1 per mil.

Variability in sea surface temperature (SST) is also driven by upwelling, advection, and heat fluxes across the air-sea interface. However, the difference in air-sea equilibration timescales for SST and $\Delta^{14}C$ differ by more than an order of magnitude. Thus the water which upwells along the equator and along the coast of Peru can retain its low isotopic signature for several years, long after it has thermally equilibrated with the atmosphere.

Paper number 96JC03604.
0148-0227/97/96JC-03604$09.00

The seasonal variability in $\Delta^{14}C$ recorded by corals needs to be understood within the context of both the large-scale surface currents of the equatorial Pacific and the bomb-$\Delta^{14}C$ transient. Away from boundaries, the most prominent circulation features in the equatorial Pacific are the zonal equatorial currents (namely Figure 1a; also see *Tomczak and Godfrey* [1994, p. 119]), namely the South Equatorial Current (SEC) between 2°S and 4°N, the North Equatorial Counter Current (NECC) between 4° and 9°N, and the North Equatorial Current (NEC) between 10° and 20°N. These currents exhibit significant seasonal variability.

Elevated atmospheric $\Delta^{14}C$ produced by weapons testing in the late 1950s and early 1960s caused two important changes in the $\Delta^{14}C$ of surface waters of the Pacific Ocean. First, the annual mean $\Delta^{14}C$ of surface waters increased by more than 150 per mil. Second, this increase was not spatially uniform. The difference between the $\Delta^{14}C$ minimum corresponding to equatorial upwelling and the $\Delta^{14}C$ maximum corresponding to convergence in the subtropical gyres was accentuated as the bomb-$\Delta^{14}C$ entered the surface ocean. Thus both the lateral and vertical gradients in upper ocean $\Delta^{14}C$ increased significantly between the 1950s and the Pacific Geochemical Ocean Sections Study (GEOSECS) surveys of the 1970s.

Previous modeling studies [*Toggweiler et al.*, 1989b, 1991; *Duffy et al.*, 1995] have addressed $\Delta^{14}C$ in the Pacific using fully three-dimension ocean circulation models, but these coarse resolution global ocean model studies focused on simulating the decadal-scale bomb-$\Delta^{14}C$ transient. In fact, *Toggweiler et al.* [1989b] forced their circulation model with climatological annual mean winds and heat fluxes at the sea surface, and thus the model circulation fields did not include seasonal changes in circulation. *Duffy et al.* [1995] included seasonal forcing but did not address the seasonal variability of $\Delta^{14}C$. Their analysis focused on a comparison of their results to GEOSECS $\Delta^{14}C$ measurements. *Druffel* [1987] used a box model to study seasonal sea surface $\Delta^{14}C$ variability in the 1970s and found cross-equatorial advection to be responsible for the variability she measured in corals from Canton and Fanning.

Model Description

Model Equations

The ocean circulation model used for this study is a nonlinear primitive equation GCM (the governing equations are given by *Gent and Cane* [1989]), which employs a sigma vertical coordinate. We use the hybrid mixed layer model of *Chen et al.* [1994a] which has been embedded in the Gent and Cane model. The hybrid model uses both a Kraus-Turner type mixed layer model [*Kraus and Turner*, 1967] and a *Price et al.* [1986] dynamical instability model to represent vertical mixing. Thus the thickness of the model's surface layer varies seasonally with changes in the surface buoyancy and momentum forcing. It has been shown to improve the Gent and Cane model's simulation of SST and circulation fields [*Chen et al.*, 1994b, and *Murtugudde et al.*, 1996].

To explore the sensitivity of $\Delta^{14}C$ variability to the model's treatment of vertical mixing, runs employing a constant thickness surface layer of 50 m were performed with the same circulation model. If seasonal mixed layer entrainment/detrainment of water were to be an important source of variability in sea surface $\Delta^{14}C$, then this process would be resolved by the variable depth mixed layer run. In addition, if the seasonal changes in currents were to be sensitive to the model's representation of vertical mixing, then this in turn could influence the tracer distribution. Hereafter we will refer to the model runs which use a variable depth mixed layer as the VML case and runs with a constant thickness surface layer as the CML case.

The model runs considered here do not include salinity, so that density is a function of temperature only. It has been shown in many modeling studies [e.g. *Chen et al.*, 1994a] that the density distribution of the equatorial thermocline is to first order controlled by the temperature distribution, so that salinity behaves as a passive tracer in the domain of our modeling study.

Artificial solid boundaries have been imposed at 30°N and 30°S, as well as at 124°E and 70°W. The boundary condition at all lateral boundaries is no normal flow. The model employs a reduced-gravity assumption and uses six vertical layers in the upper 200 m of the water column. The horizontal resolution is 1° zonally, and the meridional resolution ranges from 1° near the northern and southern boundaries to 0.333° between 10°N and 10°S. The circulation model is forced at the ocean surface by monthly Florida State University (FSU) climatological winds [*Goldenberg and O'Brien*, 1981] and by relaxing sea surface temperature to climatological monthly temperatures [*Levitus and Boyer*, 1994] on a timescale of 50 days.

In choosing 1/3° meridional resolution for our model runs, we follow a rule of thumb in numerical methods: Approximately six grid points are required to resolve a feature. As the scale width of the equatorial undercurrent is approximately 2° latitude, 1/3° resolution is needed to resolve it in a model. It is also true that 1/3° resolution will be necessary to adequately simulate upwelling and realistic advective flow fields for the equatorial Pacific.

The advection-diffusion equation for a generic tracer A is given by

$$\frac{dA}{dt} = \nabla\cdot(\kappa\nabla A) + S_o - S_i \qquad (1)$$

where κ is diffusivity and S_o and S_i represent sources and sinks. The derivative on the left-hand side of (1) is a total derivative and thus contains advective terms. The

layer integrated form of (1) that is used for advection in this model is

$$\frac{\partial(h_k A_k)}{\partial t} = -(h_k \vec{u}_k)\cdot\nabla A_k - A_k \nabla\cdot(h_k \vec{u}_k) - w_{k-1/2}A_{k-1/2} + w_{k+1/2}A_{k+1/2} + [\kappa_{k+1/2}\frac{(A_{k+1} - A_k)}{\Delta z_{k+1/2}} - \kappa_{k-1/2}\frac{(A_k - A_{k-1})}{\Delta z_{k-1/2}}] + h_k [S_o - S_i] \quad (2)$$

where the index k refers to the vertical level, and k-1/2 and k+1/2 correspond to the layer interfaces above and below, respectively. The value used for the background vertical eddy diffusivity κ in the model is about 0.1 cm^2/s, which is in accord with observations [*Ledwell et al.*, 1993]. Horizontal mixing occurs via a fourth-order Shapiro filter [*Shapiro*, 1970], and is significantly less than the typical Laplacian diffusion commonly used in ocean models. The effective diffusivity of the fourth-order Shapiro filter is

$$(\Delta x)^4/\Delta t \quad (3)$$

where Δx is the horizontal resolution and Δt is the time interval between filtering events. The meridional diffusivity along the equator, where the grid spacing is 1/3° (37 km), is 1.4 x 10^{14}m^4/s. The zonal diffusivity along the equator, where the resolution is 1° (111 km), is 1.4 x 10^{16}m^4/s.

The horizontal derivatives are approximated by a centered fourth-order discretization [*Gent and Cane*, 1989], and tracer concentration $A_{k+1/2}$ is defined at the layer interfaces as

$$A_{k+1/2} = \frac{h_k A_k + h_{k+1} A_{k+1}}{h_k + h_{k+1}} \quad (4)$$

This formulation of the advection equation is conservative of both tracer content and tracer variance [*Gent and Cane*, 1989].

We are focusing on Δ^{14}C variability which occurs on the timescale of a seasonal cycle, roughly an order of magnitude faster than the process of air-sea isotopic equilibration via gas exchange. Thus our investigation of the processes responsible for seasonal variability amounts to evaluating the relative contributions of the first three terms on the right-hand side of the following equation:

$$\frac{\partial A_1}{\partial t} = -\vec{u}_1\cdot\nabla A_1 + \frac{w_{3/2}(A_{3/2} - A_1)}{h_1} + F_v + [S_o - S_i] \quad (5)$$

where A_1 represents Δ^{14}C in the surface mixed layer, and F_v is vertical mixing. The variables $w_{3/2}$ and $A_{3/2}$ are the vertical velocity and the isotopic ratio, respectively, at the interface between the first two layers in the vertical. This equation is equivalent to (2).

The model's surface circulation fields can be verified against the monthly equatorial Pacific surface current climatology of *Reverdin et al.* [1994]. This gridded data set, whose annual mean zonal velocities are shown in Figure 1a, was constructed from data collected between January 1987 and April 1992 using drifters drogued at 15 m depth. The dataset represents the currents at 15 m depth, while the model currents are the mean values for the mixed layer. The horizontal resolution of this data set is 5° longitude by 1° latitude. It resolves seasonal variations in the currents as well as the mean, which is useful for validating the variability generated by the model. The data set of *Reverdin et al.* [1994] is appropriate for validation of models whose meridional resolution is 1° or finer in the vicinity of the equator.

Initial Distribution of Δ^{14}C in the Model

The treatment of Δ^{14}C in our tracer equation follows that of *Toggweiler et al.* [1989a], whereby surface mixed layer Δ^{14}C values are relaxed to atmospheric values on a timescale of 7.5 years per 50 m of mixed layer thickness. For the VML case, this amounts to 0.15 years per meter of mixed layer depth. The atmospheric value is held steady for each of the runs considered here, and it is assumed that biological effects are secondary to physical effects and may be neglected. For both the VML and CML model runs, we maintain the constant value $(\Delta^{14}C)_{atm}$ = 300 per mil throughout the run, consistent with atmospheric Δ^{14}C levels in the late 1970s.

The initial Δ^{14}C distribution is chosen such that the deep ocean waters have Δ^{14}C = -200 per mil, and increase linearly to Δ^{14}C = 60 per mil at 200 m depth. The mixed layer value is Δ^{14}C = 100 per mil with values decreasing linearly from the base of the mixed layer to 200 m depth. This distribution is intended to represent to first order the vertical gradients which existed for Δ^{14}C in the equatorial Pacific in the 1970s. The atmospheric value of Δ^{14}C was held steady for each of the runs considered here. This simplification omits the bomb transient, allowing a focus on our principal interest here, the mean seasonal cycle.

For each experiment, the ocean was spun up from rest for 5 years, after which the tracer field was initialized. Subsequently, the model was integrated for 15 more years. The discussion which follows focuses on the tracer field 11 years after tracer initialization. Eleven years is long enough for air-sea equilibration of carbon isotopes to create sufficiently realistic lateral gradients in sea surface Δ^{14}C within the model. For longer runs, one needs to exercise caution for transient tracer studies with a tropical domain model given the decadal exchange timescale in the real ocean between the tropics and midlatitudes.

Results

Model Circulation Fields

The mean zonal surface currents are shown in Figures 1b and 1c for the VML and CML runs, respectively.

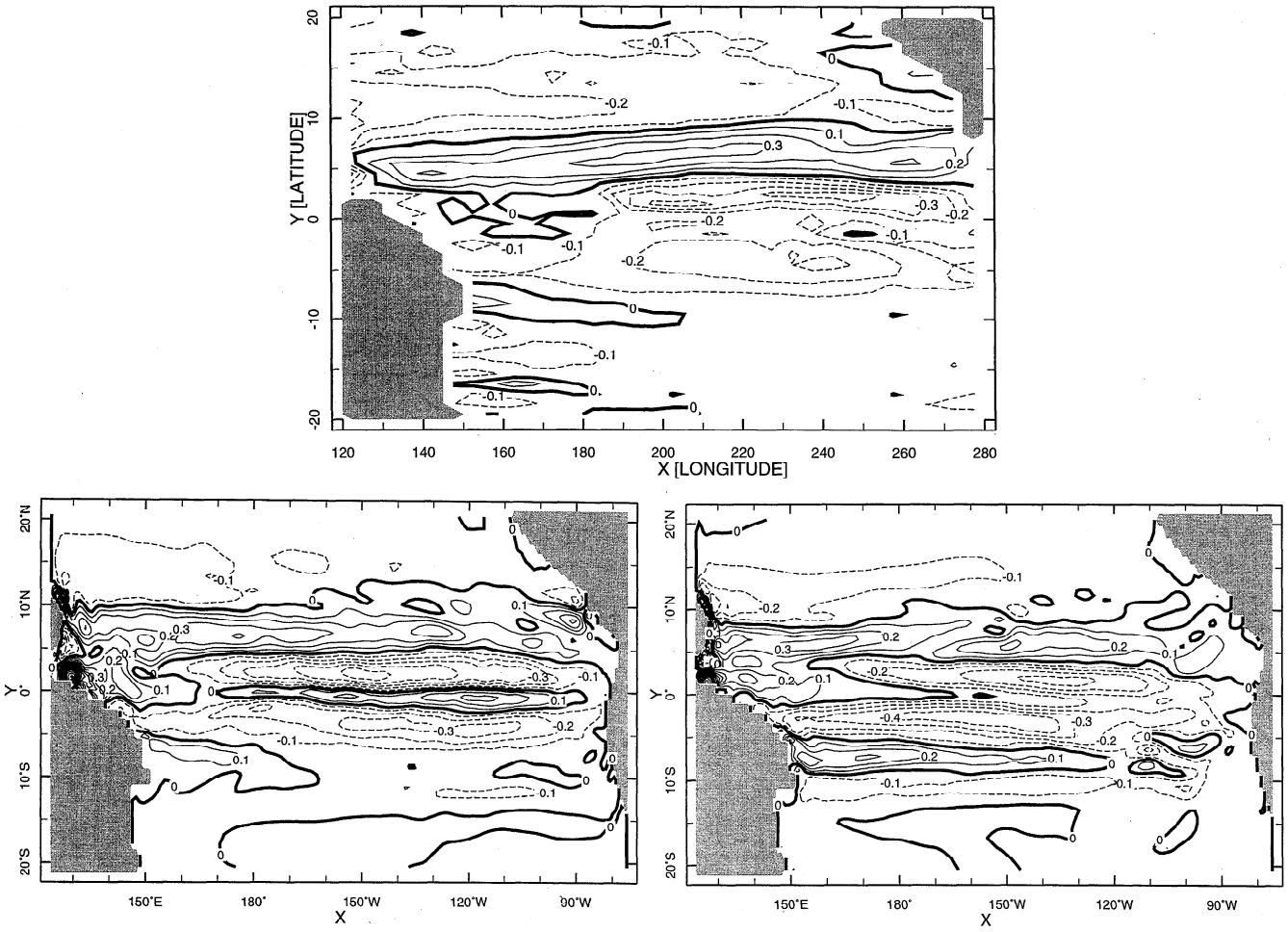

Figure 1. Annual Mean surface zonal current in meters per second (a) at 15-m depth in the equatorial Pacific, according to the drifter-derived climatology of Reverdin et al. [1994], (b) for the surface layer in the VML run, and (c) for the surface layer of the CML run. Positive values are associated with eastward currents, while negative values are associated with westward flow.

Although there are differences between these two cases, namely that the current speeds tend to be slightly larger with a constant thickness surface layer, the overall patterns for the zonal equatorial currents are quite similar.

An important feature of the model's annual mean circulation in the western Pacific is that the SEC waters which lie to the north of the equator do not penetrate to the western boundary. They feed the NECC by turning northward near the date line. We shall see that this plays an important role in establishing a large zonal gradient in $\Delta^{14}C$ for the equatorial Pacific. This circulation feature is consistent with the drifter-derived zonal current shown in Figure 1a, where the westward flowing SEC at 2°N only penetrates to 160°E.

For both the VML and CML cases, a significant portion of the NEC turns southward upon reaching the western boundary to feed the Mindanao Current, which flows equatorward along the western boundary from 12°N. Before reaching the equator, the model's Mindanao Current turns eastward to feed the NECC. In the real ocean, much of the Mindanao Current transport feeds the Indonesian throughflow and is therefore not recirculated within the Pacific. Since the model domain has a no-flux boundary condition along its western boundary, the model flow field (Figures 1b and 1c) within 15° of the western boundary is slightly distorted (compare Figure 1a) as a consequence of closing off the Indonesian throughflow.

The model currents in the open ocean are in good agreement with observations. One should keep in mind that the climatological wind stress data used to force ocean models are on a data grid which is coarser than the model grid we have chosen for this study. Thus the latitudes maintained by the model's currents should not be expected to be accurate to better than 1°.

In the southern hemisphere of the real ocean, that part of the SEC which is to the south of the equator turns to the south upon reaching the western boundary (i.e., the coast of New Guinea), where it feeds a weak South Equatorial Countercurrent (SECC) in the annual mean. The VML case is in better agreement with the *Reverdin et al.* [1994] than is the CML case in that its SECC does not penetrate east of the date line in the annual mean.

Another significant difference between the VML and CML flow fields is apparent in the annual mean zonal velocity along the equator (not shown). The undercurrent

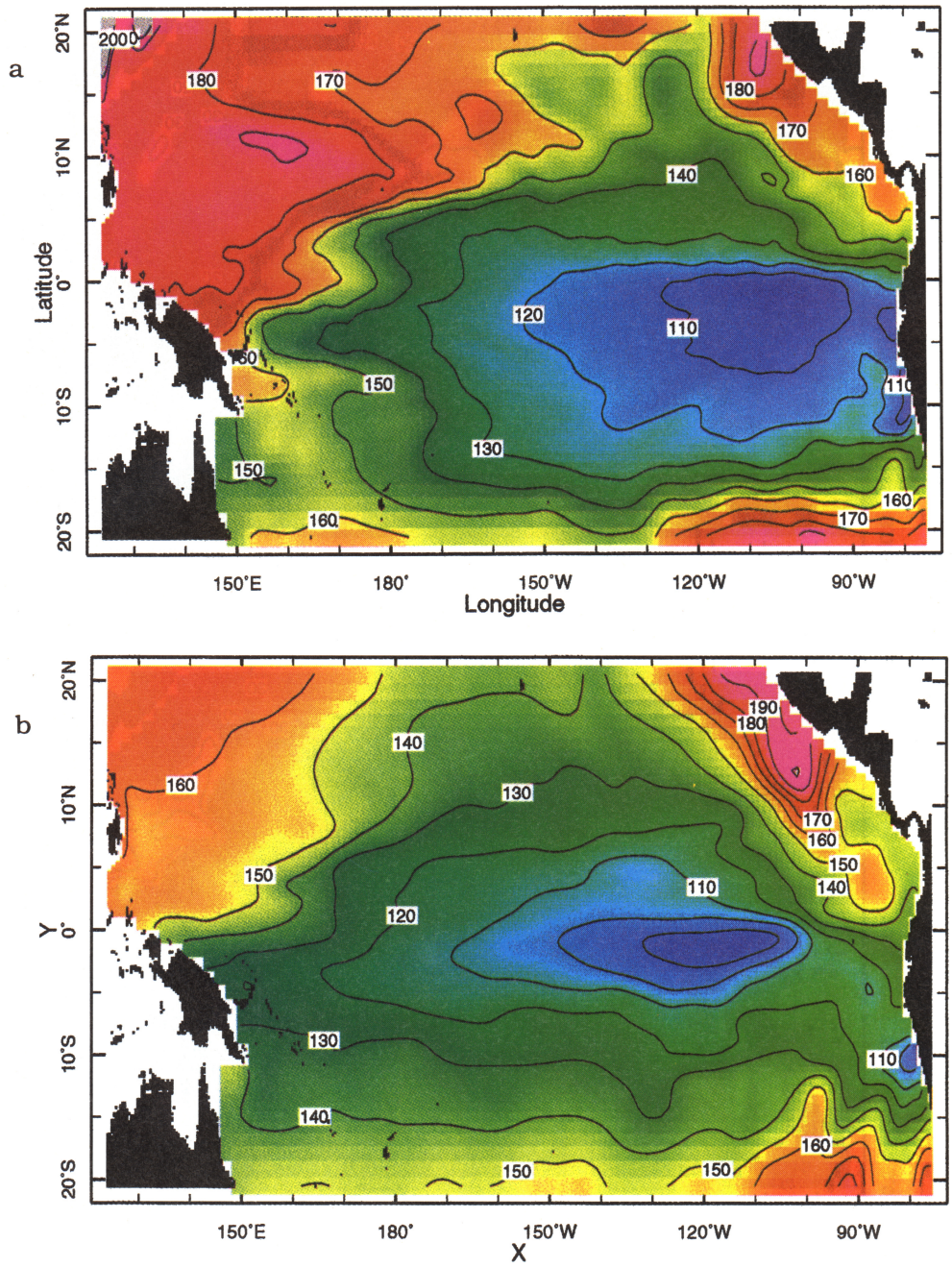

Plate 1. Annual mean (a) sea surface Δ^{14}C for the VML case, and (b) sea surface Δ^{14}C for the CML case.

is stronger for the VML case, and it penetrates much closer to the eastern boundary, in better agreement with observations, as has been pointed out by *Chen et al.* [1994b].

Structure of Annual Mean Surface Δ^{14}C Distribution

A plot of sea surface Δ^{14}C averaged over the eleventh year of the VML model integration is shown in Plate 1a. The time-averaged Δ^{14}C distribution is established by the basin-scale circulation patterns and helps to illustrate the pathways by which different water masses interact and mix in the surface ocean.

We see in Plate 1a that sea surface Δ^{14}C increases westward and poleward of the upwelling regions of the eastern and central equatorial Pacific. The initial Δ^{14}C depended on depth only, with Δ^{14}C = 100 per mil at the surface, and was thus spatially uniform. As the atmospheric forcing Δ^{14}C is also spatially uniform, the asymmetries in the Δ^{14}C distribution are revealing of the asymmetries in the circulation field. In the eastern equatorial Pacific, there is a Δ^{14}C front just north of the equator, whereas to the south of the equator, there is a more gradual transition from low-Δ^{14}C waters to high-Δ^{14}C waters. We shall see that this pool of low-Δ^{14}C water south of the equator has its source in the

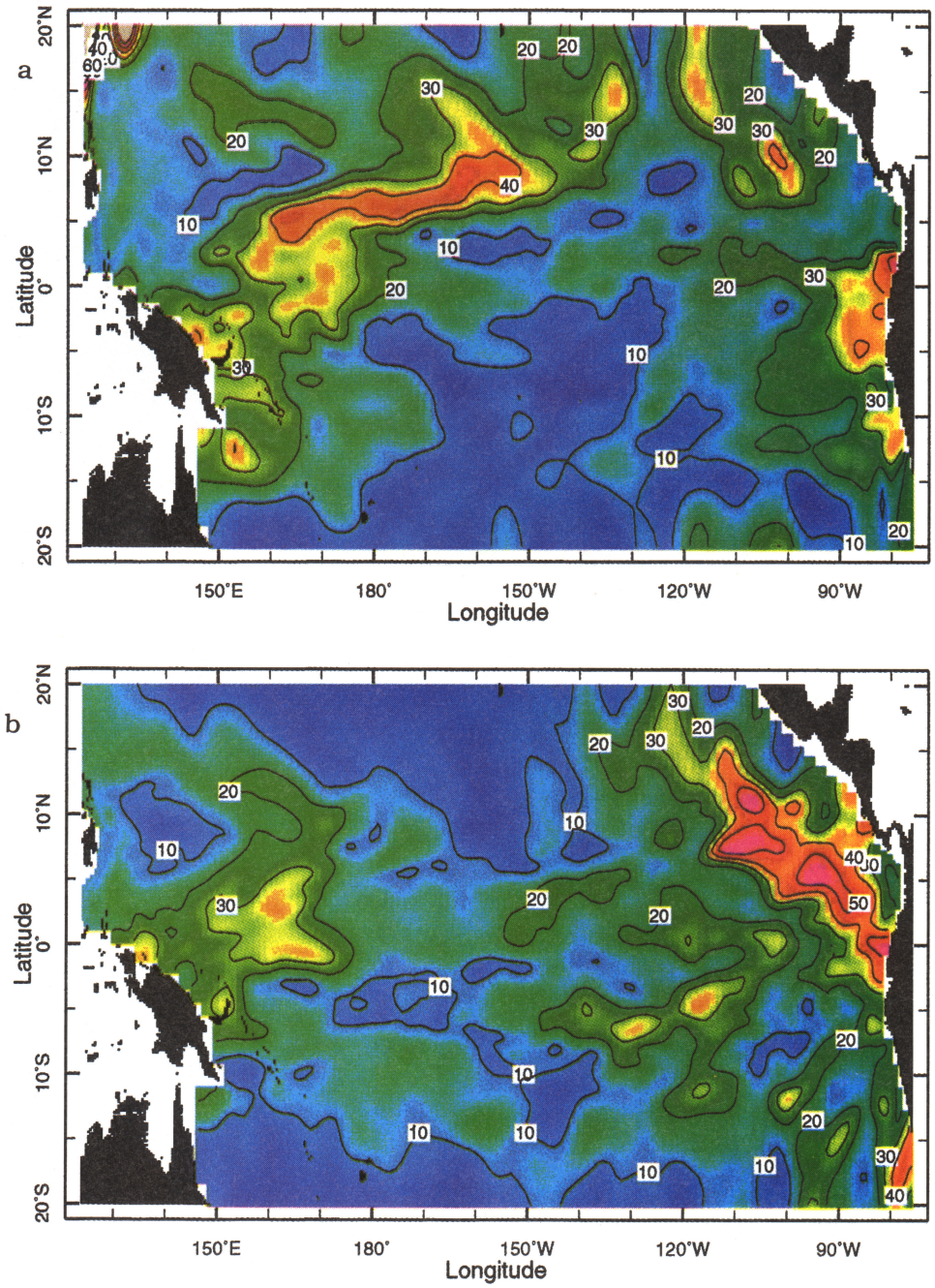

Plate 2. Maximum $\Delta^{14}C$ minus minimum $\Delta^{14}C$ for the eleventh year of model integration for (a) the VML case and (b) the CML case. Units are per mil.

narrow band of equatorial upwelling. The asymmetry in $\Delta^{14}C$ about the equator has an analog in the annual mean distribution of SST (Figure 2).

On the other hand, the asymmetries in the sea surface $\Delta^{14}C$ in the western Pacific do not have an analog in SST. The SST is nearly uniform in the western Pacific warm pool because the surface forcing is so uniform, while water in the northwest is isotopically heavier than the water in the southwest. This reflects the model flow fields: the primary water mass source for the northwest region is the NEC, while the surface waters in the southwest are fed by the South Equatorial Current in the annual mean, which brings the low-$\Delta^{14}C$ waters upwelled in the eastern equatorial Pacific across the basin.

If we compare the model's sea surface $\Delta^{14}C$ with surface Pacific GEOSECS measurements [*Ostlund and Stuiver*, 1980], we see that the model and GEOSECS are in disagreement regarding the zonal gradient in sea surface $\Delta^{14}C$. Whereas the model shows a zonal gradient of 80 per mil across the equatorial Pacific, surface GEOSECS measurements on the equator at 179°E (71.9 per mil) and 125°W (72.6 per mil) are identical to within measurement error. We will return to this point in the discussion section.

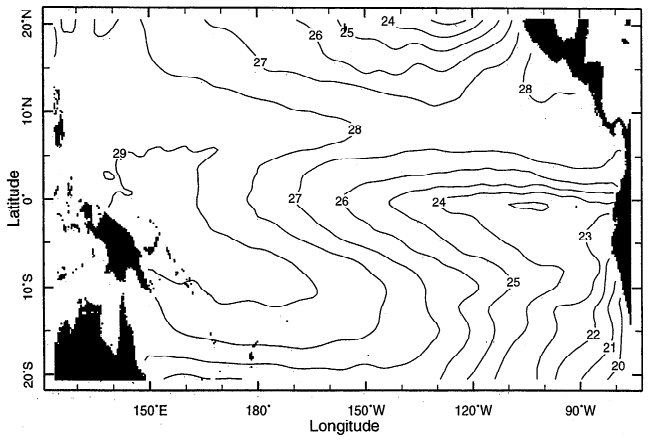

Figure 2. SST for the eleventh year of the model run for the VML case.

Next consider the sea surface $\Delta^{14}C$ distribution averaged over the eleventh year of model integration for the CML run (Plate 1b). The $\Delta^{14}C$ minimum in the Eastern Pacific is more confined to the equatorial upwelling region than it was for the VML case, where the low $\Delta^{14}C$ signal in the annual mean extended all the way to the eastern boundary (Plate 1a) and was more pronounced. Thus the distribution of the $\Delta^{14}C$ minimum is more symmetric about the equator for the constant depth mixed layer case. The absolute values of the $\Delta^{14}C$ minimum are also lower for the CML case than for the VML case.

For both the VML and CML model runs, a patch of high-$\Delta^{14}C$ surface water appears in both the northeast and southeast regions of the domain. This is an artifact of our no-flux boundary condition on the model flow fields at 30°N and 30°S. One consequence of this may be a somewhat diminished low-$\Delta^{14}C$ signature for the Peru upwelling.

For our future $\Delta^{14}C$ simulations, the model domain will be extended meridionally so as to eliminate this problem. As these high-$\Delta^{14}C$ features are confined to the model's northeastern and southeastern coastal boundaries, its effects are local to those regions and its influence can otherwise be ignored for the region of interest for our study, namely the open equatorial Pacific Ocean.

Seasonal $\Delta^{14}C$ Variability

Plate 2a shows the spatial distribution of the seasonal difference $(\Delta^{14}C)_{max}$-$(\Delta^{14}C)_{min}$ at each horizontal grid point in the model's surface layer for the eleventh year of the VML run. This plot does not reveal the phase of the variability. Regions of high seasonal variability are associated mainly with regions of large lateral gradients in the annual mean sea surface $\Delta^{14}C$, as can be seen by comparison with Plate 1a. In the neighborhood of 170°E, to the north of the equator, the region of highest variablity coincides with the boundary between the high-$\Delta^{14}C$ waters to the west and the low-$\Delta^{14}C$ water mass to the east. The central equatorial Pacific is relatively quiescent as far as seasonal $\Delta^{14}C$ variability is concerned.

Figure 3 shows sea surface $\Delta^{14}C$ for the VML case as a function of longitude and time at four latitudes, 13°N, 5°N, 0°N, and 5°S. The latitudes 5°N and 13°N are chosen because they are representative of the model's NECC and NEC at the date line (compare Plate 1a), whereas 0°N is representative of the SEC.

Each of these plots shows the changes in $\Delta^{14}C$ along a constant latitude line from the end of the tenth year of model integration to the end of the thirteenth year. As expected, the system has not yet reached steady state, and annual mean $\Delta^{14}C$ values continue to slowly rise over this 3-year interval.

At 13°N (Figure 3a), we can see the effect of a relatively constant advection rate between 120°W and 150°E. Low-$\Delta^{14}C$ equatorial water, which appears seasonally at 120°W (note the penetration of low-$\Delta^{14}C$ water into the latitude belt of the NEC in the annual mean at 120°W in Plate 1a), is advected to the west, and it eventually reaches 150°E nearly 2 years later.

At 5°N (Figure 3b), there is significant variability between 150° and 180°E, which correlates with the strength of the NECC; at times when the NECC is strong, high-$\Delta^{14}C$ water is advected in from the west. The phase and the amplitude of the variability of the model's NECC are consistent with the phase and amplitude of the *Reverdin et al.* [1994] current climatology. Unlike the pattern at 13°N, where the isolines reflected uniform advection to the west, the $\Delta^{14}C$ isolines at 5°N oscillate zonally by as much as 20° longitude on a seasonal timescale. For example, the $\Delta^{14}C$ = 160 isoline in Figure 3b reaches furthest to the east between October and December. By February the $\Delta^{14}C$=160 isoline has shifted to its westernmost longitude. At 165°E, the seasonal variability is as large as 40 per mil.

Along 0°N, there is also significant variability to the west of the date line (Figure 3c). As was the case at 5°N, there is an oscillatory pattern to the isolines centered around 165°E. Variability in that region is as large as 40 per mil, with the highest values occurring in December and January and the lowest values occurring in April. There is also variability as large as 40 per mil near the eastern boundary along the equator, which is associated with the meridional excursions of the $\Delta^{14}C$ front apparent in the annual mean surface distribution of $\Delta^{14}C$ (see Plate 1a).

The seasonal variability at 5°S (Figure 3d) is significantly smaller than the variability at 5°N in the western Pacific; for example, at 165°E, the seasonal variability is less than 10 per mil. In the eastern Pacific, however, the variability is as high as 50 per mil at 90°W, 5°S. The $\Delta^{14}C$ values are lowest in September and highest in March.

For the CML case, the difference $(\Delta^{14}C)_{max}$-$(\Delta^{14}C)_{min}$ for the eleventh year is shown in Plate 2b. The amplitude of the seasonal variability in the region bounded by

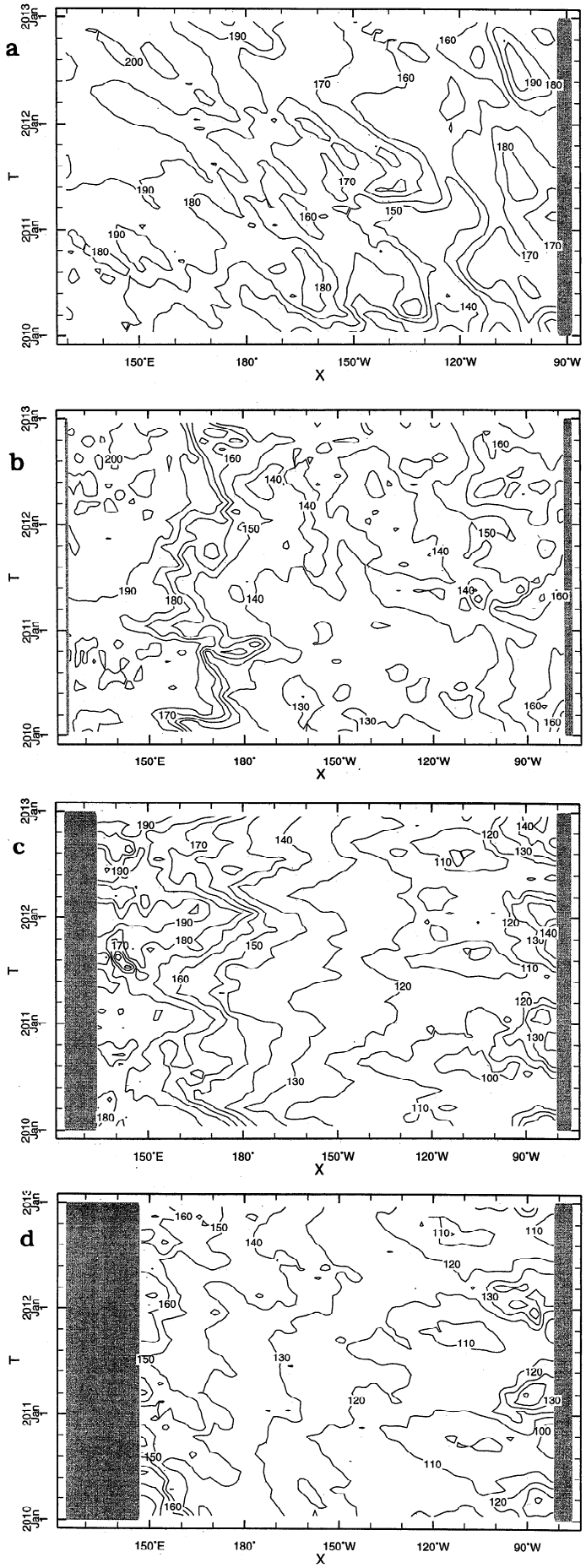

150°E, 180°E in longitude and 5°S, 10°N in latitude is as large as 40 per mil, consistent with our results for the VML case. Once again, this is a region of large lateral $\Delta^{14}C$ gradients, and the mechanism for seasonal $\Delta^{14}C$ variability is seasonally varying lateral advection.

In the eastern Pacific a ring of variability of magnitude 20 to 40 per mil exists between 140° and 100°W, surrounding the $\Delta^{14}C$ minimum associated with upwelling. This is also due to seasonal varying lateral advection. Within this ring $\Delta^{14}C$ variability is negligible. Further to the west between 180°E and 150°W, where the lateral gradients in sea surface $\Delta^{14}C$ are quite small, the seasonal $\Delta^{14}C$ variability is low.

Discussion

Model Circulation Fields

The mean distribution of $\Delta^{14}C$ in the surface ocean is largely determined by the annual mean surface currents. The 80 per mil zonal $\Delta^{14}C$ gradient across the equatorial Pacific is the difference between the high-$\Delta^{14}C$ water supplied to the western equatorial region from the north by the Mindanao Current and the low-$\Delta^{14}C$ water upwelled in the eastern equatorial Pacific. We attributed seasonal variability in $\Delta^{14}C$ (Plate 2) to the seasonal variability of the zonal currents. Now we compare the seasonal changes for the VML model run with the seasonal changes in the current data of *Reverdin et al.* [1994] at two representative longitudes in the equatorial Pacific.

The first of these is in the region of maximum $\Delta^{14}C$ variability to the west of the date line at 165°E. In Figure 4a, which shows zonal velocity as a function of latitude and time, we see that the model's surface current along the equator is highly variable. In fact, the current undergoes strong seasonal reversals. This is consistent with the *Reverdin et al.* [1994] current climatology (Figure 4b), which shows westward flow in March and April in excess of 20 cm/s, with eastward flow of the same magnitude in November and December. When the model's eastward flow is strongest during December and January, high-$\Delta^{14}C$ water is being advected in from the west. Likewise, when the flow is westward in March, low-$\Delta^{14}C$ water is being advected from the upwelling region to the east. By comparison with Figure 1b, we see that the annual mean flow field at this location is very nearly zero, which is also consistent with the *Reverdin et al.* drifter data shown in Figure 1a.

Between 5° and 10°N at 165°E (Figure 4a), we see that the eastward flowing NECC also experiences seasonal variability, which is consistent with the drifter data set at this longitude. The NECC in the real ocean is

Figure 3. Variability in sea surface $\Delta^{14}C$ at four latitudes for the VML case, beginning 10 years into the model run: (a) 13°N, (b) 5°N, (c) 0°N, and (d) 5°S.

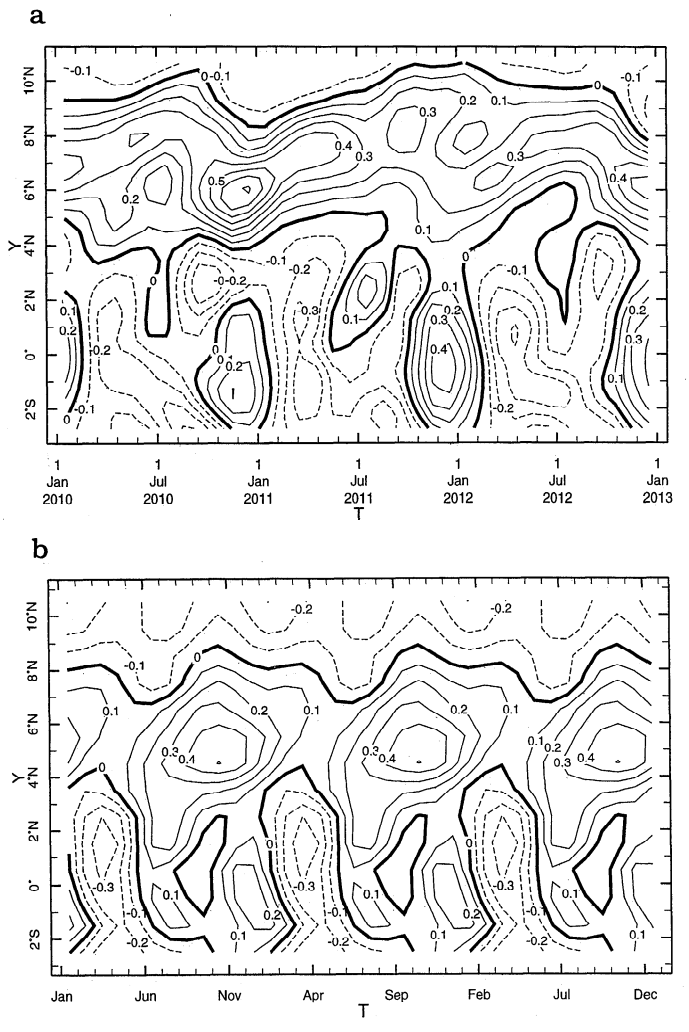

Figure 4. Variability in zonal velocity at 165°E according to (a) the VML case and (b) the Reverdin et al. [1994] climatology. The contouring interval is 0.1 m/s, and positive values are associated with eastward flow.

strongest in September (Figure 4b), when the ITCZ is in its northernmost position. It appears that the phase in the model's NECC is lagging by a few months at this longitude.

The second longitude at which we consider seasonal changes in zonal velocity is at 92°W, in the vicinity of Galapagos. In August and September (the latter part of austral winter), as well as during January and February, the flow along the equator is to the west (Figure 5a shows the model results, and the drifter data are shown in Figure 5b). In March and April, on the other hand, the current reverses and flows to the east against the prevailing SEC. This occurs at a time when the local wind forcing is relatively weak, and the equatorial undercurrent surfaces.

In fact, the seasonal reversal of the current along the equator for the VML case is one of the causes of the asymmetry seen in Δ^{14}C in Plate 1a for the eastern Pacific. The strong eastward flow associated with the surfacing of the undercurrent brings low-Δ^{14}C water to the east of Galapagos, where it turns south and floods the region between 0°N and 10°S with low-Δ^{14}C water. The CML case does not experience such a reversal and thus does not produce this asymmetry. The difference in the parameterization of vertical mixing between the VML and the CML cases thus has important nonlocal effects on the mean surface Δ^{14}C distribution.

Structure of Annual Mean Surface Δ^{14}C Distribution

The 80 per mil zonal gradient in sea surface Δ^{14}C across the equatorial Pacific for the VML case is consistent with Δ^{14}C gradients inferred from annual growth bands of corals across the equatorial Pacific from the late 1970s. *Druffel* [1987] found the annually averaged Δ^{14}C of Galapagos corals (1°S, 90°W) to be roughly 40 per mil in the late 1970s, while *Konishi et al.* [1982] found the Δ^{14}C of corals from Ponape (7°N, 158°E) from the same period to be of order 130 per mil. Taken together, these two coral measurements indicate a zonal gradient in Δ^{14}C of 90 per mil across the equatorial Pacific,

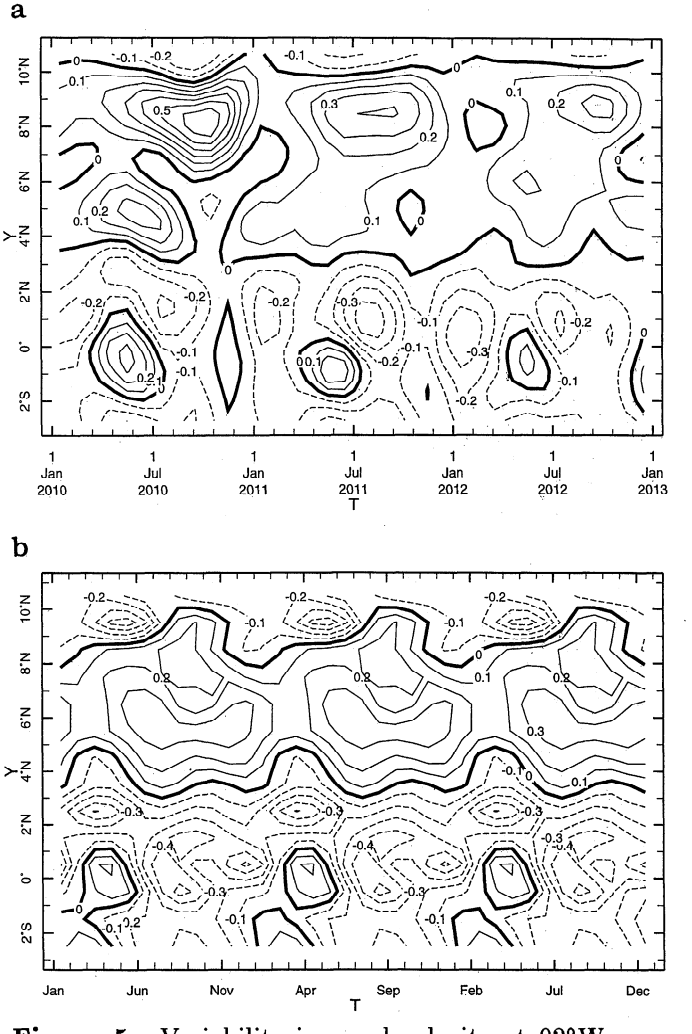

Figure 5. Variability in zonal velocity at 92°W according to (a) the VML run and (b) the Reverdin et al. [1994] climatology.

which is nearly as large as the equator-to-midlatitude meridional gradients measured during GEOSECS in the Pacific.

The zonal gradient in $\Delta^{14}C$ according to both our model and the annually averaged corals is larger than that measured during GEOSECS, according to which, there was almost no zonal gradient across the equator in the Pacific. GEOSECS measurements along 179°E were made in December of 1973, and measurements along 125°W were made during May and June of 1974. Significant seasonal and interannual variability in sea surface $\Delta^{14}C$ can lead to a significant seasonal bias in measurements along cruise transects, since these measurements represent a "snapshot" of surface conditions. Thus GEOSECS aliased the seasonal cycle and interannual variability into their sampling. Repeat stations in the Atlantic during GEOSECS [*Broecker and Peng*, 1980] as well as mixed layer measurements over broad regions of the North Pacific between 1984 and 1989 [*Takahashi et al.*, 1991] indicate that 30 to 50 per mil seasonal variability of sea surface $\Delta^{14}C$ during the 1970s and 1980s was not limited to the tropical Pacific.

A separate experiment was conducted to test the sensitivity of the model's sea surface $\Delta^{14}C$ gradients to the value chosen for $(\Delta^{14}C)_{atm}$. This run was identical to the VML case except that we used $(\Delta^{14}C)_{atm} = 600$ per mil. The pattern of the $\Delta^{14}C$ isolines is nearly identical to the pattern for the VML case (Plate 1a), where we used $(\Delta^{14}C)_{atm} = 300$ per mil. The amplitude of the lateral gradients in sea surface $\Delta^{14}C$, as well as the amplitude of the seasonal variability, scales nearly linearly with the value chosen for $(\Delta^{14}C)_{atm}$. This can be seen in Figure 6a, which shows the sea surface $\Delta^{14}C$ as a function of time for the VML case at 90°W, 0°N, and Figure 6b, which shows the sea surface $\Delta^{14}C$ as a function of time for the VML case at 165°E, 0°N, The value used for $(\Delta^{14}C)_{atm}$ could be chosen to get the annual mean zonal gradient in sea surface $\Delta^{14}C$ correct in the model, but this would not guarantee that the amplitude of the seasonal variability would also be correct. However, our argument is that the two of them are connected, and our ability to get both the gradient and the seasonal variability together is consistent with our idea that seasonal variability in lateral advection is responsible for the observed variability.

We mentioned in the previous section that the seasonal reversal of the current along the equator in the eastern equatorial Pacific contributes to the asymmetry of $\Delta^{14}C$ about the equator in the annual mean. There is an upwelling of low $\Delta^{14}C$ waters along the coast of Peru near 10°S which also contributes to the asymmetry. *Toggweiler et al.* [1991] concluded from their modeling study that the upwelling off of Peru was responsible for the asymmetry. However, their coarse resolution model run, which was forced with annual mean momentum and heat fluxes at the sea surface, was unable to resolve all of the relevant physical processes which could contribute to an asymmetry in the distribution of $\Delta^{14}C$ about the equator. In particular, it does not resolve the scales necessary to adequately capture equatorial upwelling.

Given that the initial $\Delta^{14}C$ distribution is a function of depth only, our model simulation does not allow us to distinguish the water which upwells along the equator from water which upwells along the coast of Peru. Since the Peru upwelling is from deeper in the thermocline than the equatorial upwelling, the $\Delta^{14}C$ of surface water in the real ocean can be used to distinguish these two upwelling sources. As mentioned earlier, high-$\Delta^{14}C$ levels which are associated with the artificial boundary at 30°S may also diminish the imprint of the Peru upwelling on sea surface $\Delta^{14}C$. In a future study we will address this issue by using a more realistic initial condition for $\Delta^{14}C$ and by using a domain with greater latitudinal extent.

The annual mean sea surface $\Delta^{14}C$ minimum is lower for the CML case (Plate 1b) than for the VML case (Plate 1a). Although the undercurrent is stronger for the VML case, the low-$\Delta^{14}C$ signature of upwelled waters in the mixed layer along the equator is diluted by the seasonal reversal in the zonal current along the equator. The absence of a seasonal reversal for the CML case results in a lower annual mean $\Delta^{14}C$ along the equator than is found for the VML case.

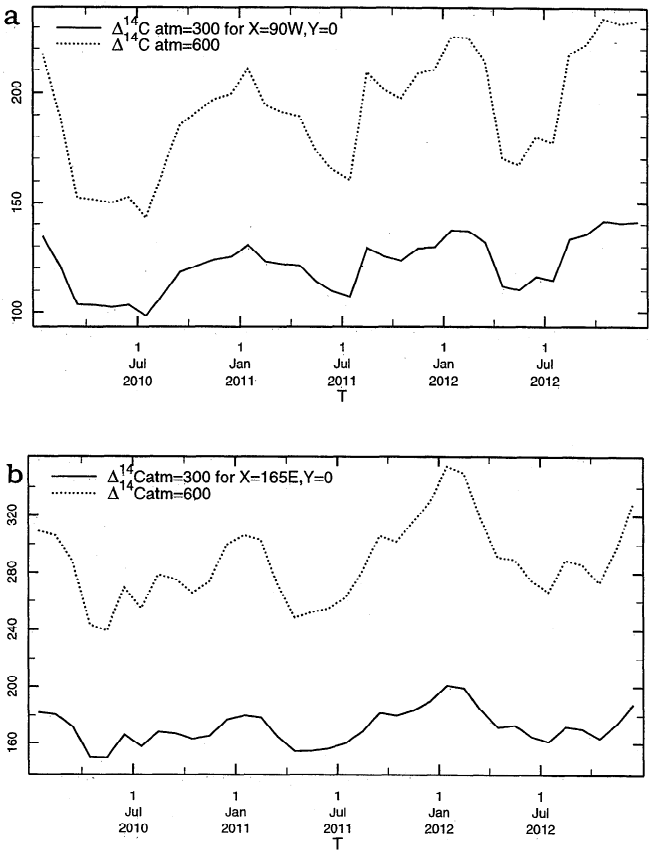

Figure 6. $\Delta^{14}C$ as a function of time in the surface layer at (a) 90°W, 0°N and (b) 165°E, 0°N. For both cases, the response to atmospheric forcing which uses $(\Delta^{14}C)_{atm} = 300$ per mil and $(\Delta^{14}C)_{atm} = 600$ is shown.

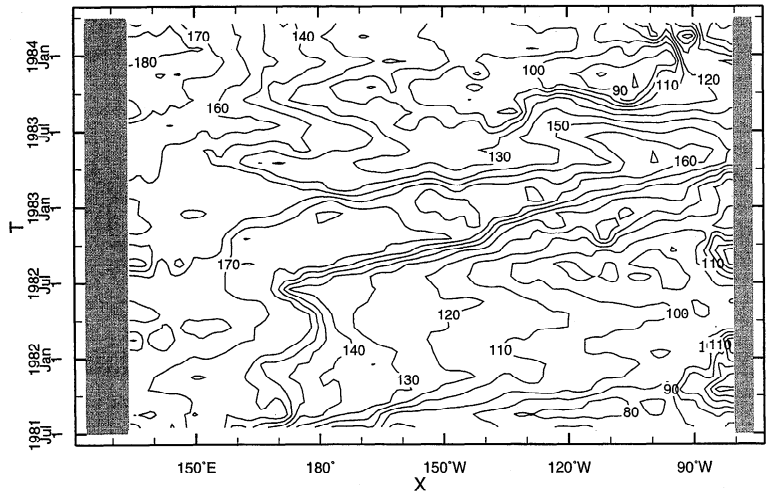

Figure 7. For a model run forced with interannual winds (FSU), the variability in Δ^{14}C as a function of longitude and time along 0°N is shown. Unlike the seasonally forced case (Figure 8c), where the Δ^{14}C isoline is confined to the western Pacific, here it is advected all the way to the eastern boundary during the 1983 El Niño. As with the seasonally forced case, here we have chosen simplified initial conditions and forcing, so the patterns are more significant that the absolute numbers.

Seasonal Δ^{14}C Variability

The seasonal variability of Δ^{14}C along 13°N should be understood within the context of the pathways by which equatorial and NEC waters are exchanged meridionally across 10°N. Between 120° and 150°W in the eastern Pacific, there is a seasonal poleward transport of low-Δ^{14}C equatorial water across 10°N. This penetration of low-Δ^{14}C water into the latitude belt of the NEC is a pronounced feature in the annual mean sea surface Δ^{14}C shown in Plate 1a, as characterized by the water mass with Δ^{14}C<150 per mil. This is caused by the relatively strong trade winds in this region in January and February which drive an increased poleward Ekman drift across 10°N between 120° and 150°W. This is consistent with the seasonally varying poleward heat flux identified by *Philander and Hurlin* [1988] for this same region. The westward advection of this low Δ^{14}C water mass from 135°W to 150°E can be seen in Figure 3a. Despite the fact that it takes more than a year for a water parcel to be advected from 135°W to 150°E within the NEC, it retains its low-Δ^{14}C signature. Thus the seasonal variability in Δ^{14}C to the west of the date line along 13°N is in large part due to seasonal poleward surges of low-Δ^{14}C equatorial surface water across 10°N into the NEC thousands of kilometers to the east. There is also a contribution from local meridional advective processes in the western Pacific, which act in phase with the variability associated with the NEC itself.

Interannual Δ^{14}C Variability

In addition to the runs which were seasonally forced, we performed an experiment with the FSU interannual wind field [*Goldenberg and O'Brien*, 1981] to study the effect of the wind stresses associated with the 1982-1983 El Niño on the sea surface Δ^{14}C distribution of the Equatorial Pacific. As with the VML run, this experiment uses the vertical mixing scheme of *Chen et al.* [1994a], as well as $(\Delta^{14}C)_{atm}$ = 300 per mil, and the same initial distribution of Δ^{14}C in the ocean.

Tracer initialization occurs in 1971, and by 1981 the annual mean sea surface Δ^{14}C is much like that shown for the seasonally forced case shown in Plate 1a. The sea surface Δ^{14}C as a function of longitude and time along the equator between 1981 and 1984 is shown in Figure 7. Whereas in Figure 3c (the seasonally forced VML case) the Δ^{14}C = 160 isoline moves approximately 20° longitude between 155° and 175°E on seasonal timescales, we see in Figure 7 that between July 1982 and March 1983 the Δ^{14}C = 160 isoline travels from 170°E to 90°W. Thus the signal is advected more than 100° longitude within the equatorial waveguide and appears in the region of Galapagos as a high-Δ^{14}C anomaly.

It has been shown that both the seasonal and interannual components of sea surface Δ^{14}C variability are significant and are capable of changing the zonal gradient of Δ^{14}C across the equatorial Pacific on timescales of several months. Seasonal variability in ocean circulation alone is unlikely to account for all of the aliasing, as the phasing of the results of the seasonally forced model run shown in Figure 6 suggest that for measurements made in the western Pacific during December 1973 and in the eastern Pacific during May 1974, the zonal gradient in sea surface Δ^{14}C should be enhanced rather than diminished. We believe that the discrepancy in the phasing can be accounted for by interannual variability in ocean circulation on ENSO timescales. In a future simulation of the bomb-Δ^{14}C transient for the Pacific,

we will address the interannual component of the variability explicitly. Our point here was to show that it exists and that it can be significant.

As with the seasonal case, the interannual experiment represents a process study, since we have used the same simplified initial conditions and atmospheric forcing. Thus it is the shapes of the $\Delta^{14}C$ contours rather than their absolute magnitudes which are significant. The advection of high $\Delta^{14}C$ waters to the east within the waveguide is consistent with observations of freshwater anomalies of warm pool origin observed in the eastern Pacific during El Niño [*Kessler and Taft*, 1987; *Picaut and Tournier*, 1991].

Concluding Remarks

A primitive equation ocean circulation model, forced with seasonally varying momentum and heat fluxes at the sea surface, and using simplified initial conditions and forcing for $\Delta^{14}C$, is capable of generating significant seasonal variability in sea surface $\Delta^{14}C$ for the equatorial Pacific. Our results indicate that seasonal variability of the surface currents is the dominant mechanism for $\Delta^{14}C$ variability. Upwelling and air-sea exchange play essential supporting roles in establishing the large-scale horizontal gradients in sea surface $\Delta^{14}C$. Low-resolution models lose the advective mechanism for $\Delta^{14}C$ variability because they can not resolve the narrow equatorial currents or the critical features of equatorial upwelling.

Seasonal variability in $\Delta^{14}C$ is largest in our model for regions where there are strong lateral gradients in sea surface $\Delta^{14}C$. One such region is the western Pacific in a box bounded by 150° and 180°E zonally and 3°S and 15°N meridionally. Another region is in the eastern Pacific near 90°W. For both of these regions, the large seasonal variability in $\Delta^{14}C$ is due to seasonal migration of nearby surface $\Delta^{14}C$ fronts due to seasonally varying lateral advection.

Interestingly, the equatorial upwelling region between 160° and 120°W shows very little seasonal variability but potentially large interannual variability within the equatorial waveguide. The interannual variability in this region is due to the advection of high-$\Delta^{14}C$ water from further west. It is our hope that modeling studies such as this one will be of value to those who make coral measurements in choosing their sampling sites.

These model runs represent a process study, as they use simplified initial conditions and forcing for $\Delta^{14}C$. Thus although it was not our intention to simulate the coral records, the increased variability measured at Galapagos during the 1972-1973 El Niño [*Brown et al.*, 1993] is not inconsistent with our model results which provide an advective mechanism whereby anomalously high $\Delta^{14}C$ water can reach Galapagos.

Future work will investigate the role of the Indonesian throughflow on $\Delta^{14}C$. Estimates for the magnitude of the Indonesian throughflow in the real ocean are in the range 0-20 Sv [*Lukas et al.*, 1996]. Thus a sizeable fraction of the Mindanao Current water (with an estimated transport of 20-35 Sv) will flow to the Indian Ocean. The sensitivity of the model's $\Delta^{14}C$ distribution to an open flow condition around Australia will be investigated.

Our motivation for running both the variable-depth mixed layer (VML) and constant depth mixed layer (CML) cases was to assess the contribution of entrainment to the variability. We found that although the seasonal variability is slightly higher for the VML case than for the CML case, this is only partially due to local entrainment and detrainment associated with changes in mixed layer thickness on seasonal timescales. Rather, the difference in the parameterization of vertical mixing for the VML and CML cases led to differences in currents along the equator, where there is large vertical shear. These differences in turn caused differences in the $\Delta^{14}C$ distributions of the two cases. We see that the parameterization of vertical mixing in primitive equation models has far reaching nonlocal consequences in $\Delta^{14}C$ distributions.

Acknowledgments. We would like to thank Senya Basin and Naomi Naik for their support with the ocean model and Gilles Reverdin for his helpful comments. This work was supported by National Science Foundation contract number OCE 93-02613. This is Lamont-Doherty Earth Observatory contribution 5675.

References

Broecker, W. S., and T. H. Peng, Seasonal variability in the $^{14}C/^{12}C$ ratio for surface ocean water, *Geophys. Res. Lett.*, *7*, 1020-1022, 1980.

Brown, T., G. Farwell, P. Grootes, F. Schmidt, and M. Stuiver, Intra-annual variability of the radiocarbon of corals from the Galapagos islands, *Radiocarbon*, *35*, 245-251, 1993.

Chen, D., L. M. Rothstein, and A. J. Busalacchi, A hybrid vertical mixing scheme and its application to the tropical ocean, *J. Phys. Oceanogr.*, *24*, 2156-2179, 1994a.

Chen, D., A. J. Busalacchi, and L. M. Rothstein, The Roles of Vertical Mixing, Solar Radiation, and Wind Stress in a Model Simulation of the Sea Surface Temperature Seasonal Cycle in the Tropical Pacific Ocean, *J. Geophys. Res.*, *99*, 20,345-20,359, 1994b.

Druffel, E., Bomb radiocarbon in the Pacific: Annual and seasonal timescale variations, *J. Mar. Res.*, *19*, 35-46, 1987.

Duffy, P., D. Eliason, A. Bourgeois, and C. Covey, Simulation of bomb radiocarbon in two global ocean general circulation models, *J. Geophys. Res.*, *100*, 22,545-22,563, 1995.

Gent, P. R., and M. A. Cane, A reduced gravity, primitive equation model of the upper equatorial ocean, *J. Comput. Phys.*, *81*, 444-480, 1989.

Goldenberg, S. B., and J. J. O'Brien, Time and space variability of tropical Pacific wind stress, *Mon. Weather Rev.*, *109*, 1190-1205, 1981.

Gu, D., and S.G.H. Philander, Interdecadal Climate Fluctuations that depend on exchanges between the tropics and the extratropics. *Science*, *275*, 805-807, 1997.

Kessler, W., and B. A. Taft, Dynamic heights and zonal

geostrophic transports in the central tropical Pacific during 1979-84, *J. Phys. Oceanogr.*, *17*, 97-122, 1987.

Konishi, K., T. Tanaka, and M. Sakanoue, Secular variation of radiocarbon concentration in seawater: Sclerochronological approach, in *Proceedings of the Fourth International Coral Reef Symposium*, vol. 1, edited by E. D. Gomez, pp. 181-185, Mar. Sci. Cen., Univ. of the Philippines, Manila, 1982.

Kraus, E. B., and J. S. Turner, A one-dimensional model of the seasonal thermocline. II: The general theory and its consequences., *Tellus*, *19*, 98-106, 1967.

Ledwell, J., A. Watson, and C. Law, Evidence for slow mixing across the pycnocline from an open-ocean tracer-release experiment, *Nature*, *364*, 701-703, 1993.

Levitus, S., and T. P. Boyer, *World Ocean Atlas 1994*, vol. 4, *Temperature*, 117 pp., U.S. Dep. of Comm., Washington, D. C., 1994.

Lukas, R., T. Yamagata, and J. McCreary, Pacific low-latitude western boundary currents and the Indonesian throughflow. *J. Geophys. Res.*, *101*, 12,209-12,216, 1996.

Moore, M., D. Schrag, and M. Kashgarian, Coral radiocarbon constraints on the source of the Indonesian throughflow, *J. Geophys. Res.*, *102*, 12,359-12,365, 1997.

Murtugudde, R., R. Seager, and A. Busalacchi, Simulation of tropical oceans with an ocean GCM coupled to an atmospheric mixed layer model, *J. Clim.*, *9*, 1795-1815.

Ostlund, H., and M. Stuiver, GEOSECS Pacific radiocarbon, *Radiocarbon*, *22*, 25-53, 1980.

Philander, S., and W. Hurlin, The heat budget of the tropical Pacific Ocean in a simulation of the 1982-83 El Niño, *J. Phys. Oceanogr.*, *18*, 926-931, 1988.

Picaut, J., and R. Tournier, Monitoring the 1979-1985 equatorial Pacific current transports with expendable bathythermograph data, *J. Geophys. Res.*, *96*, 3263-3277, 1991.

Price, J., R. Weller, and R. Pinkel, Diurnal Cycle: Observations and models of the upper ocean response to diurnal heating, cooling, and wind mixing, *J. Geophys. Res.*, *91*, 8411-8427, 1986.

Reverdin, G., C. Frankignoul, E. Kestenare, and M. McPhaden, A climatology of the seasonal currents in the equatorial Pacific, *J. Geophys. Res.*, *99*, 20,323-20,344, 1994.

Shapiro, R., Smoothing, filtering, and boundary effects, *Rev. Geophys.*, *8*, 359-387, 1970.

Takahashi, T., J. Goddard, D. Chipman, S. Sutherland, and G. Mathieu, Assessment of CO_2 Sink/Source in North Pacific Ocean: Seasonal and Geographic Variability, 1984-1989, Final Technical Report to DOE for Contract 19X-SC428C, Lamont Doherty Geol. Observ., Palisades, N.Y., 111 pp., 1991.

Toggweiler, J. R., K. Dixon, and K. Bryan, Simulations of radiocarbon in a coarse-resolution, world ocean model, I, Steady state, pre-bomb distribution, *J. Geophys. Res.*, *94*, 8217-8242, 1989.

Toggweiler, J. R., K. Dixon, and K. Bryan, Simulations of radiocarbon in a coarse-resolution, world ocean model, II, Distribution of bomb-produced ^{14}C, *J. Geophys. Res.*, *94*, 8243-8264, 1989.

Toggweiler, J. R., K. Dixon, and W. S. Broecker, The Peru upwelling and the ventilation of the South Pacific thermocline, *J. Geophys. Res.*, *96*, 20,467-20,497, 1991.

Tomczak, M., and J. S. Godfrey, *Regional Oceanography: An Introduction*, 422 pp., Elsevier Science, New York, 1994.

M. A. Cane and K. B. Rodgers, Lamont-Doherty Earth Observatory of Columbia University, Palisades, New York 10964. (e-mail: keithr@ldeo.columbia.edu and mcane@ldeo.columbia.edu)

D. P. Schrag, Department of Geological Sciences, Princeton University, Princeton, NJ 08544-1003. (e-mail: schrag@geo.princeton.edu)

(Received December 8, 1995; revised November 6, 1996; accepted November 12, 1996.)